

ONERA



Tiré à Part

Simulation of the 3D unsteady flow in a slat cove for noise prediction

*M. Terracol, E. Labourasse, E. Manoha, P. Sagaut**

9th AIAA/CEAS Aeroacoustics Conference & Exhibit
Hilton Head (USA), May 12-14, 2003

TP 2003-62

Simulation of the 3D unsteady flow in a slat cove for noise prediction

Simulation de l'écoulement tridimensionnel instationnaire dans une cavité de bord d'attaque
pour la prévision acoustique

par

*M. Terracol, E. Labourasse, E. Manoha, P. Sagaut**

* Université Paris VI, LMM, 8 rue du Capitaine Scott, F-75008 Paris

9th AIAA/CEAS Aeroacoustics Conference & Exhibit
Hilton Head (USA), May 12-14, 2003

Résumé : Ce papier décrit certaines avancées vers la simulation numérique du bruit rayonné par les dispositifs hypersustentateurs des avions. La simulation numérique complète d'une telle configuration étant toujours hors de portée des supercalculateurs actuels, des stratégies hybrides ont été développées pour réduire le coût global de telles simulations.

La première stratégie repose sur l'emploi d'une méthode hybride RANS/LES. Cette méthode permet de réduire de manière significative le coût d'une prévision numérique précise des sources de bruit instationnaires en réduisant considérablement l'étendue spatiale de la zone LES. Cette méthode est décrite et appliquée à la simulation numérique de l'écoulement tridimensionnel instationnaire dans une cavité de bord d'attaque d'un profil hypersustenté.

La seconde stratégie repose sur le couplage d'une simulation CFD instationnaire avec un solveur de propagation acoustique basé sur la résolution des équations d'Euler. La méthode numérique d'ordre élevé requise pour la propagation est détaillée, et une application de cette méthode de couplage à la prévision numérique du bruit d'un profil NACA0012 bidimensionnel à bord de fuite effilé est présentée.

Simulation of the 3D Unsteady Flow in a Slat Cove for Noise Prediction

M. Terracol ^{*}, E. Labourasse [†], E. Manoha ^{*}

ONERA, BP 72, 29 av. de la division Leclerc, 92322 Châtillon Cedex, France

P. Sagaut [‡]

Université Paris VI, LMM, 8 Rue du Capitaine Scott 75008, Paris, France

This paper describes some significant steps towards the numerical simulation of the noise radiated by the high-lift devices of a plane. Since the full numerical simulation of such configuration is still out of reach for present supercomputers, some hybrid strategies have been developed to reduce the overall cost of such simulations. The first strategy relies on the use of a hybrid RANS/LES method. This method allows to reduce significantly the cost of an accurate numerical prediction of the unsteady noise sources by reducing considerably the extent of the LES zone. This method is described and applied to the numerical simulation of the three-dimensional unsteady flow in the slat cove of a high-lift profile. The second strategy relies on the coupling of an unsteady nearfield CFD simulation with an acoustic propagation solver based on the resolution of the Euler equations. The high-order numerical method required for the propagation solver is detailed, and an application of this coupling method to the numerical sound prediction of a two-dimensional NACA0012 airfoil with sharp trailing-edge is presented.

Introduction

THE general context of this paper is the numerical prediction of the aerodynamic noise generated by the high lift devices - HLD, slats and flaps - of large airliners, an important contributor to the total radiated airframe noise, especially in approach configuration. It is commonly admitted that the design of new low-noise HLD concepts incorporating specific noise reduction devices, although still relying on necessary experiments, will take growing advantage of the numerical simulation in terms of lower costs and shorter delays, especially considering the spectacular continuing progress of Computational AeroAcoustics (CAA) methods. The problem of the numerical simulation of HLD noise is still beyond the capabilities of complete Direct Numerical Simulation (DNS), so hybrid methods are used in most practical cases. In previous studies (see^{1,2} for instance), a three-step hybrid method has been presented and successfully applied to the farfield noise simulation of a NACA0012 airfoil with blunted trailing edge. The proposed method was based on the coupling of: i/ a nearfield 3D unsteady LES to provide an accurate description of the aerodynamic noise sources ; ii/ a midfield sound propagation step on an inhomogeneous flow by the use of a numerical propagation solver based on the resolution of the Euler equations under a perturbation form ; iii/

a farfield noise prediction step by the use of integral methods such as Kirchhoff integration, where the flow is homogeneous.

The aim of the present study is to apply a similar methodology to simulate the aerodynamic noise generated by a high-lift wing configuration. The first step of the hybrid method is to get an accurate description of the unsteady aerodynamic sources by the mean of a 3D unsteady simulation of the flow near the wing profile. Such a simulation is still away from the numerical capabilities of "usual" supercomputers. We thus have chosen to perform only some zonal computations close to the main elements responsible of sound generation. This study focusses on an accurate simulation of the turbulent flow in the slat cove region of a high-lift wing. The local 3D unsteady simulation is performed by the mean of a zonal hybrid RANS/LES approach developed by Labourasse and Sagaut.³

One possible CFD/CAA hybrid process, based on the coupling between a DNS/LES solver and an Euler propagation solver is also presented. A first application to the full noise prediction of the flow around a 2D NACA0012 airfoil is presented.

The paper is organized as follows: first, the hybrid RANS/LES method is detailed. Particular attention is devoted to the boundary conditions used to perform some local simulations. The method is then successfully applied to the unsteady three-dimensional simulation of the flow in the slat cove of a high-lift wing profile, revealing the existence of several flow features responsible of noise generation. The second part of the paper is devoted to the hybrid CFD/CAA coupling method. After describing the global numer-

^{*}Research Engineer, ONERA, CFD and Aeroacoustics Department

[†]PhD student, ONERA, CFD and Aeroacoustics Department

[‡]Professor, Laboratoire de Modélisation pour la Mécanique and ONERA

ical method, the high-order numerical schemes used to compute the spatial derivatives are detailed. The application of a full-integrated CFD/CAA hybrid process to the NACA0012 configuration is then presented. The last part of the paper draws our main conclusions, and discusses our future orientations.

All the computations presented in this paper have been carried out using the in-house SABRINA solver (Solver for Aeroacoustics of BRoadband INteractions from Aerodynamics).

Hybrid RANS/LES method

For a large overview of this method, the reader is referred to the works by Labourasse and Sagaut.³

Basic equations

We consider the compressible Navier-Stokes equations under the following compact form:

$$\frac{\partial U}{\partial t} + \mathcal{N}(U) = 0 \quad (1)$$

where $U = (\rho, \rho \mathbf{u}^T, \rho E)^T$, $\mathbf{u} = (u, v, w)^T$ and :

$$\mathcal{N}(U) = \begin{pmatrix} \nabla \cdot (\rho \mathbf{u}) \\ \nabla \cdot (\rho \mathbf{u} \otimes \mathbf{u}) + \nabla p - \nabla \cdot \sigma \\ \nabla \cdot ((\rho E + p)\mathbf{u}) - \nabla \cdot (\sigma : \mathbf{u}) + \nabla \cdot Q \end{pmatrix} \quad (2)$$

where p is the pressure, ρ the density, \mathbf{u} the velocity vector, and ρE the total energy. Classical expressions are used for the viscous stress tensor σ and viscous heat flux vector Q , *i.e.*:

$$\sigma = -2\mu S^d \quad (3)$$

$$Q = -\kappa \nabla T \quad (4)$$

where the exponent d denotes the deviatoric part of a tensor, T is temperature, and S is the rate-of-strain tensor:

$$S = \frac{1}{2} (\nabla \mathbf{u} + (\nabla \mathbf{u})^T) \quad (5)$$

The temperature is linked to the pressure by the perfect gas state-law, and Sutherland's law is used to compute the viscosity μ as a non-linear function of T . Finally, the thermal conductivity coefficient κ is linked to viscosity through the use of a Prandtl number assumption ($Pr = 0.7$ in this study) as: $\kappa = C_p \mu / Pr$, where C_p is the iso-pressure heat coefficient.

Flow decomposition

The method used in this study can be seen as the generalization to viscous flows of the NLDE (Non-Linear Disturbance Equations) method proposed by

Morris *et al.*⁴ The principle of the method is to decompose the field U as a mean part (Reynolds average in this study) and a fluctuating part. The mean part U_0 is then computed using a classical RANS modelisation on the whole configuration, while the calculation of the fluctuating part U' is achieved locally thanks to a LES like simulation. This decomposition is a triple decomposition of the full unsteady field U as:

$$U = U_0 + U' + U_{SGS} = \overline{U} + U_{SGS} \quad (6)$$

where $\overline{(\cdot)}$ corresponds to the LES filtering, and U_{SGS} refers to the (unresolved) subgrid scales in the LES terminology.

Perturbation equations

Starting from the full Navier-Stokes equations (1), we obtain Reynolds-averaged and LES-filtered equations by applying respectively a Reynolds-averaging operator denoted by $\langle \cdot \rangle$ and a low-pass frequency filter denoted by $\overline{(\cdot)}$.

The Reynolds-averaged equations are then:

$$\frac{\partial U_0}{\partial t} + \mathcal{N}(U_0) = \mathcal{T}_R \quad (7)$$

and the filtered equations are:

$$\frac{\partial \overline{U}}{\partial t} + \mathcal{N}(\overline{U}) = \mathcal{T}_L \quad (8)$$

where $U_0 = \langle U \rangle$ is the mean part of the full field U , and \mathcal{T}_R and \mathcal{T}_L are respectively the classical Reynolds and subgrid scale tensors which require a numerical parametrization.

The evolution equations for the perturbation field U' are then simply obtained by substrating the Reynolds-averaged equations (7) from the filtered equations (8):

$$\frac{\partial U'}{\partial t} + \mathcal{N}(U' + U_0) - \mathcal{N}(U_0) = \mathcal{T}_L - \mathcal{T}_R \quad (9)$$

It was shown in ref.³ that solving the perturbation equations (9) instead of the full filtered equations (8) allows to minimize the sensitivity of the solution to numerical errors and/or to the use of relatively coarse discretization grids. More particularly, this allows to consider some reduced domain sizes, and thus to perform a local LES coupled with a global RANS simulation. In such a simulation, the perturbation field U' appears less sensitive to the numerical treatment at the RANS/LES coupling interface than the full field U . However, a particular treatment is needed to prevent strong reflections at the interfaces, for both the unsteady turbulent structures and some acoustic waves. An extension of the characteristic theory to the perturbations has been retained as boundary condition. The derivation of such a boundary condition is described in the next section.

Boundary conditions : characteristic theory applied to the perturbation equations

Because of the reduction of the domain size, attention has to be payed to the definition of the boundary conditions and more particularly to the inflow ones. To deal with a short domain size, a non-reflecting time dependent boundary condition for the fluctuations is derived according to the characteristic theory (see⁵ for a review of this theory).

In the non-conservative form, the Navier-Stokes equations can be written :

$$\frac{\partial V}{\partial t} + A \frac{\partial V}{\partial x} + B \frac{\partial V}{\partial y} + C \frac{\partial V}{\partial z} = VIS \quad (10)$$

where $V = (\rho, u, v, w, p)^T$ is the primitive variable vector, VIS accounts for the viscosity and subgrid scales terms and A, B and C are the classical convection matrices.

V can be divided into three parts according to the NLDE decomposition:

$$V = V^0 + V' + V^{SGS} \quad (11)$$

The first part, $V^0 = (\rho_0, u_0, v_0, w_0, p_0)^T$, deals with the statistically mean field, while the second part is connected with the fluctuating field $V' = (\rho', u', v', w', p')^T$.

As in all the other works dealing with the subject, the contribution of the subgrid scale term V^{SGS} will be neglected in the following characteristic analysis.

This leads to the following equation for the fluctuating field:

$$\frac{\partial V'}{\partial t} + A \frac{\partial V'}{\partial x} + B \frac{\partial V'}{\partial y} + C \frac{\partial V'}{\partial z} = VIS' - \left(\frac{\partial V^0}{\partial t} + A \frac{\partial V^0}{\partial x} + B \frac{\partial V^0}{\partial y} + C \frac{\partial V^0}{\partial z} - VIS_0 \right) \quad (12)$$

where VIS' and VIS_0 account respectively for the fluctuating and mean part of the viscosity terms. By analogy with the extension of the characteristic theory to the viscous flows (see⁶ for instance), only the convection terms of the fluctuations are now considered, which leads to neglect the right hand side of the equation (12).

The resulting equation is the following one:

$$\frac{\partial V'}{\partial t} + A \frac{\partial V'}{\partial x} + B \frac{\partial V'}{\partial y} + C \frac{\partial V'}{\partial z} = 0 \quad (13)$$

Classically, the matrix $E = An_x + Bn_y + Cn_z$ (where $n = (n_x, n_y, n_z)^T$ is the vector normal to the considered boundary) has now to be diagonalized in order to set conditions on the characteristic variables of the equation. We can then write:

$$\begin{aligned} \Lambda &= LEL^{-1} = \text{diag}(\lambda^1, \lambda^2, \lambda^3, \lambda^4, \lambda^5) \\ &= \text{diag}(u_n, u_n, u_n, u_n + c, u_n - c) \end{aligned} \quad (14)$$

where u_n is the projection of the velocity vector on the normal to the boundary, c is the sound velocity, and L is the matrix of the left eigenvectors.

Then, the temporal evolutions of the primitive variables ($\delta V'$) and those of the characteristic variables are linked by:

$$\delta W' = L\delta V' \quad \text{or} \quad \delta V' = L^{-1}\delta W' \quad (15)$$

where W' is the characteristic variables vector.

We can now derive a non-reflecting boundary condition for the fluctuating field following Thomson:⁷

$$\frac{\partial W^{1,2}}{\partial t} \equiv \delta W^{1,2} = \begin{cases} 0 & \text{if } \lambda_i \leq 0 \\ \frac{W^{1,2}{}_{n+1} - W^{1,2}{}_{n}}{\Delta t} & \text{if } \lambda_i > 0 \end{cases} \quad (16)$$

Numerical schemes

A second order accurate scheme has been retained for space discretization. Such a low-order scheme appears sufficient here, since the unsteady computation is local, and remains a near-body simulation. Thus, the mesh resolution appears sufficient to accurately describe the nearfield sound propagation. However, for midfield and farfield sound propagation, some higher-order schemes would be required. The possible coupling of the unsteady aerodynamic simulation with a high-order propagation solver, and the possible use of high-order schemes to compute the aerodynamic field are discussed in the last section of this paper.

The spatial scheme retained in this study is the modified AUSM+P scheme developed by Mary *et al.*⁸ This scheme takes advantage of a wiggle detector that allows to limit the numerical dissipation of the scheme to the zones where odd-even numerical wiggles are detected. Elsewhere, the scheme acts as a centered non-dissipative scheme well-suited for LES applications.

For time integration, both explicit and implicit schemes have been used:

- Explicit computations are carried out by the use of a third-order accurate low-storage Runge-Kutta scheme. Such simulations provide an accurate description of the high-frequency phenomena, but are limited to rather short physical integration times because of the small time steps used. They thus cannot provide a full description of the low-frequency phenomena occurring in the flow.

- Implicit computations are carried out with a second-order accurate scheme, based on an approximate Newton solver. The implicit temporal scheme acts as a low-pass frequency filter due to the large time steps used, but allows to perform longer simulation, and thus describe the low-frequency phenomena present in the flow.

Slat Cove Computation

This part deals with the unsteady numerical simulation of the slat cove from a high-lift wing. A three-element high-lift wing with deployed slat and flap is considered.

Configuration description

The physical parameters of this configuration are the following: the wing chord (in cruise configuration) is equal to 0.61 meters. The upstream velocity is 65.5 m/s , leading to a chord Reynolds number equal to 2.5 millions.

A steady, 2D RANS computation is first carried out over the full high-lift configuration using the Spalart-Allmaras model on a 411664 points grid.

Then, the instantaneous 3D turbulent fluctuating field is computed using the hybrid method in a small region that encompasses the slat cove (see figure 1). It is worth noting that the LES subdomain is computationally decomposed into several grid blocks.



Fig. 1 Location of the LES subdomain

The hybrid RANS/LES simulations are carried out on three dimensional meshes. The grid distribution is the same as for the RANS simulation in the (x,z)

plane (with $\sim 110,000$ points/plane). Several simulations have been performed, corresponding to different spanwise extents (2.7% and 27% of the slat chord) and/or spanwise mesh sizes (32 or 52 points). The fluctuating field is assumed to be periodic in the spanwise direction. As mentioned previously, both explicit and implicit simulations have been performed, to get a broadband description of the flow physics. In the present paper, only the results with the 27% chord extent with 52 meshpoints in the spanwise direction are presented. Indeed, simulations with the "reduced" spanwise extent of 2.7% chord have been found to remain quasi-bidimensional and thus appear not large enough to represent the transverse unstable modes.

Results analysis

First of all, it is striking that the hybrid RANS/LES computation allows to correct the mean field in comparison with the RANS approach, as it can be seen on figure 2 presenting some mean flow streamlines inside the slat cove. Two additive separation zones are indeed present in the RANS/LES result, a first one just behind the slat's trailing edge, and a more important one at the leading edge of the main wing body. This highlights the difficulties of simulating accurately this type of flow by RANS calculations. Indeed, Khorrami et al.⁹ have found necessary to switch off the model effects in the leading edge region to restore this second separation zone in their URANS computations.

An instantaneous Schlieren-like view of the field in a (x,z) plane is shown in figure 3, while the dilatation field $\Theta = \nabla \cdot \mathbf{u}$ is displayed in figure 4. This last quantity is proportional to the acoustic pressure time derivative, and thus allows to filter very low frequency oscillations. These two figures make it possible to investigate the flow structure and to observe acoustic waves propagation. Looking at them, several basic flow features are detected, which are all associated to noise emission and to specific frequencies in the pressure spectrum:

- A mixing layer develops in the shear region which bounds the main recirculating bubble on the suction side of the slat (S2). Due to strong streamline curvature effects, eddies of opposite spanwise vorticity sign are not symmetric. Pairing is also observed to occur. As seen on figure 5 presenting the acoustic spectrum obtained just behind the slat's trailing edge, the associated main frequency is 1.5 kHz , with subharmonics (due to vortex pairing), and higher-order harmonics.
- A secondary recirculation bubble is seen on the slat suction side (S1), which interacts with coherent vortices swept along the slat surface by the main recirculation. The main associated frequencies observed at this location (see fig. 6) are similar to those obtained in the mixing layer S2,

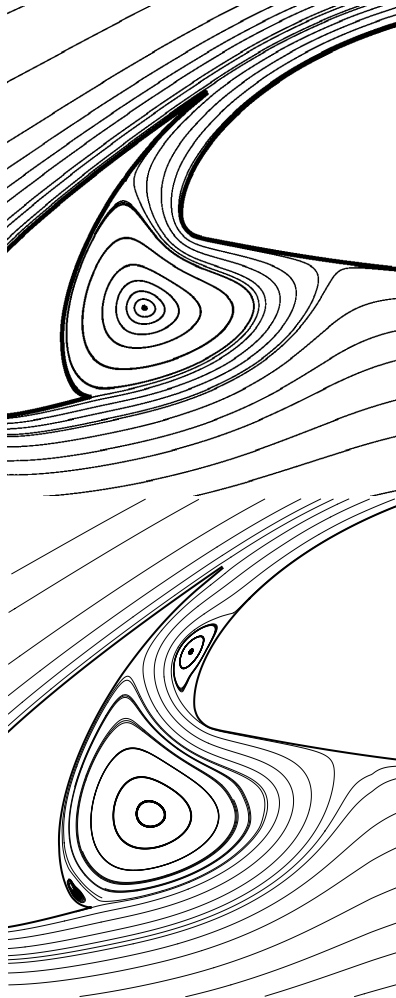


Fig. 2 Mean flow streamlines. Top : RANS computation, Bottom : Hybrid RANS/LES computation.

indicating a strong interaction between the two flow features S1 and S2.

- An important secondary turbulent recirculation bubble is observed in the fence, on the main body surface (S3). Two different phenomena occur here: a mixing layer subjected to the Kelvin-Helmholtz instability develops, with a main vortex shedding frequency about 10 kHz . An erratic, lower frequency vortex shedding is also detected, which could be explained by the interaction of the classical "breathing mode" of the recirculation bubble with the chaotic advection of coherent vortices coming from the mixing layer through the fence. Figure 7 presents the sound pressure spectrum obtained in the center of the recirculation bubble, which appears to be a full spectrum due to the high level of turbulence observed in the fence.
- The last phenomenon is the slat wake (S4). Remembering that the slat has a blunt trailing edge,

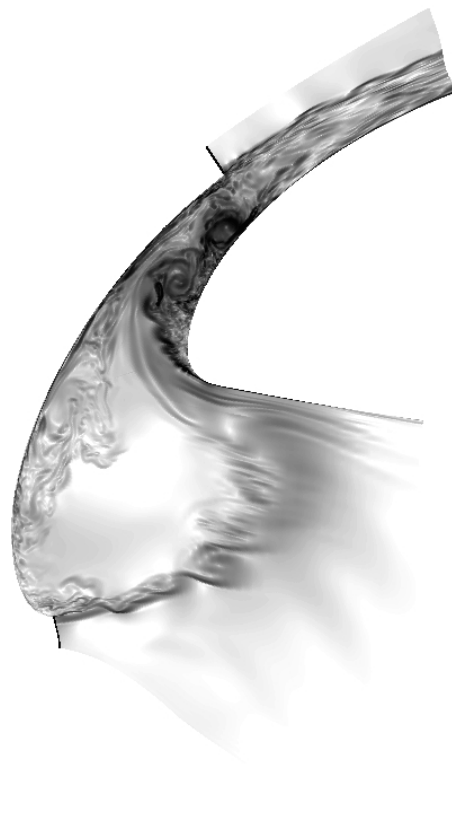


Fig. 3 Instantaneous Schlieren-like view

a coherent vortex shedding with a main frequency of about 30 kHz is detected. A more precise analysis of this flow feature alone has also been carried out by mean of a numerical simulation using a smaller computational domain localized around the slat's trailing edge. This simulation takes into account the boundary layer on the upper side of the slat, while the influence of the turbulent bubble in the fence is removed. A global view of the dilatation field obtained in this case on the full computational domain considered is shown on fig. 8. An acoustic wave pattern is clearly emitted at the trailing edge, with a frequency of about 30 kHz , as mentioned previously. This frequency is associated to the vortex shedding, and recovered on the acoustic spectrum at the trailing edge (fig. 9). In the wake, the main frequency becomes quickly of about 15 kHz (fig. 10), which is explained by the vortex pairing in the wake.

Hybrid CFD/CAA coupling method

The problem of the noise prediction of realistic configuration such as high lift devices is still beyond the field of application of Direct Noise Computation strategies, in which both the aerodynamic and acoustic fields are directly resolved by unsteady methods such as LES/DNS. Thus, hybrid CFD/CAA meth-

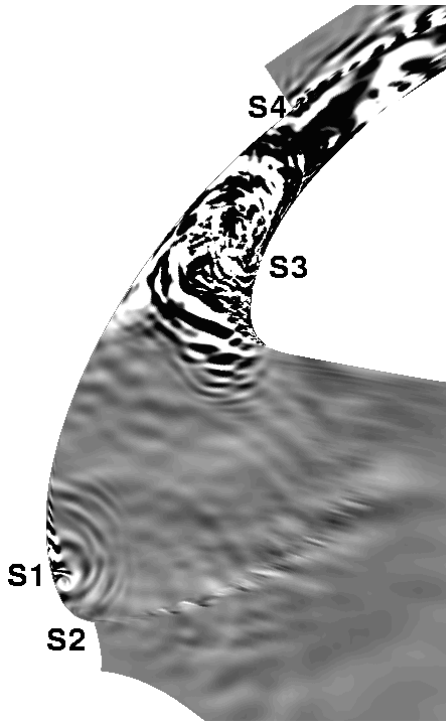


Fig. 4 Isovalue contours of the dilatation field Θ

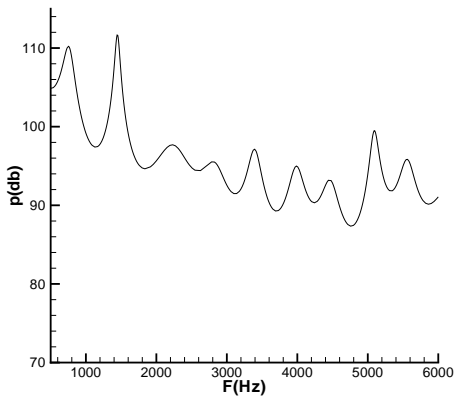


Fig. 5 Acoustic pressure spectrum at location S2

ods have to be used in most practical cases, in which the nearfield turbulent flow and the farfield noise are computed separately, using different solvers. The idea is to divide the physical space into several domains, in which specific physical mechanisms are simulated using the most adequate set of equations with the cheapest discretization strategy.

Principle of the method

Computational Fluid Dynamics techniques are first used to get an accurate prediction of the local unsteady noise sources, as for example the hybrid RANS/LES strategy presented in the previous section. This local flow solution has then to be coupled with an acoustic

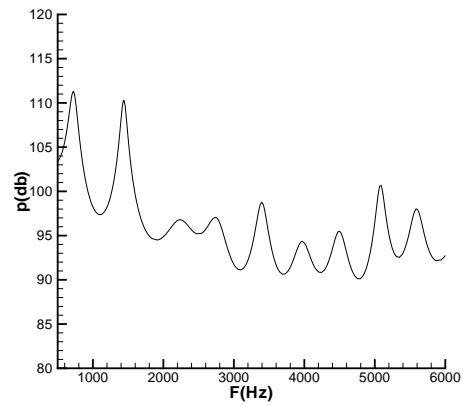


Fig. 6 Acoustic pressure spectrum at location S1

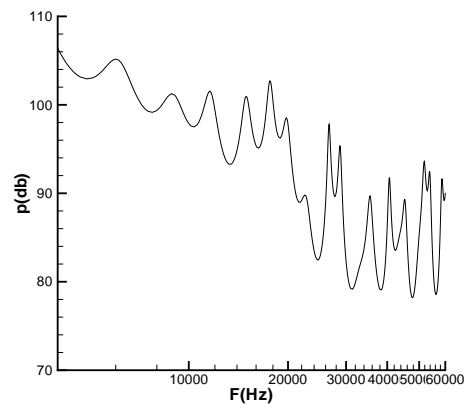


Fig. 7 Acoustic pressure spectrum in the recirculation bubble S3

numerical technique for the prediction of the mid- and farfield noise. The most practical formulations are the integral methods such as Lighthill's analogy¹⁰⁻¹² (including the Ffowcs Williams-Hawkings (FW-H) equation¹³⁻¹⁶), the Boundary Element Method (BEM)¹⁷ and the Kirchhoff integral.

Integral methods assume that, beyond a given distance from the noise sources and body surfaces, the sound propagates in a medium at rest, or moving with uniform velocity. This assumption may become a strong limitation, especially when the radiated noise results from a surface integration on a control interface which is located near solid walls, where velocity gradients are still significant. In that case, only the discretized Euler equations governing the acoustic propagation may account for the propagation in non-homogeneous flows. This is obtained at the price of a significant computational effort since the propagation domain must be meshed with an adequate resolution with respect to the smallest acoustic wavelength, and also because finite difference high order



Fig. 8 Isovalue contours of the dilatation field Θ

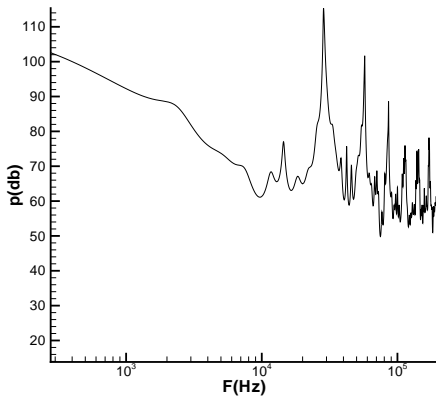


Fig. 9 Acoustic pressure spectrum at the slat's trailing edge

schemes are needed to ensure numerical accuracy and low dispersion of the propagation of acoustic waves.¹⁸ Moreover, application to realistic geometries including airfoils need curvilinear grids^{19–21} on which the use of high order schemes is not straightforward. However, the domain in which Euler equations are used can be strictly limited to regions where velocity gradients are significant : in most practical airframe noise problems, an external boundary can be found, beyond which the flow can be assumed uniform, so that integral methods can be used for the noise prediction at very long distance from the airframe.

The present part focusses on the direct coupling between a CFD solver and a propagation solver based on the resolution of the Euler equations under a perturbation form used to get a prediction of the noise radiated in the midfield. Then, this solver can be simply relayed by an integral method to get a farfield noise prediction.

The global idea of this CFD/CAA coupling is to directly inject the aerodynamic fluctuations computed

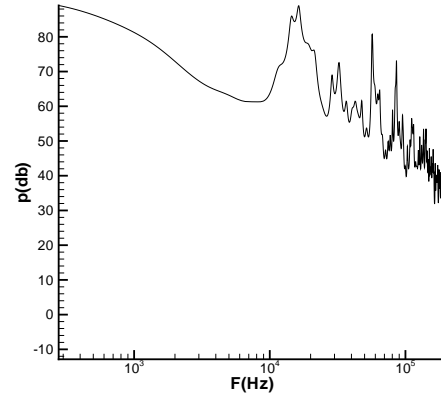


Fig. 10 Acoustic pressure spectrum in the slat's wake

in the CFD zone as an entry data for an Euler propagation zone. In this last zone, the Euler equations are solved under a perturbation form, *i.e.*:

$$\frac{\partial U'}{\partial t} + \mathcal{C}(U_0 + U') - \mathcal{C}(U_0) = 0 \quad (17)$$

where \mathcal{C} is the convective (Euler) term of the Navier-Stokes equations:

$$\mathcal{C}(U) = \begin{pmatrix} \nabla \cdot (\rho \mathbf{u}) \\ \nabla \cdot (\rho \mathbf{u} \otimes \mathbf{u}) + \nabla p \\ \nabla \cdot ((\rho E + p) \mathbf{u}) \end{pmatrix} \quad (18)$$

The resolution of this set of equations for an acoustic purpose requires the use of higher order numerical schemes than the ones generally used in the CFD context. In this study, centered finite-difference schemes have been used. These schemes are easily extensible to any order, but require a particular numerical treatment to handle curvilinear grids. The next section is devoted to the description of these schemes.

High-Order Finite-Differencing Scheme

The spatial scheme used to discretize space derivatives is based on a finite-difference centered explicit scheme. From a discrete point of view, the first order derivative of any quantity ϕ at point i (see fig. 11) is then simply evaluated as a weighted average of ϕ at the neighbouring points:

$$\left. \frac{\partial \phi}{\partial x} \right|_i \simeq \left. \frac{\delta \phi}{\delta x} \right|_i = \frac{1}{\Delta x} \sum_{k=-N}^N a_k \phi_{i+k} \quad (19)$$

In this expression, the term $1/\Delta x$ is the metric term, only valuable in the case of uniform cartesian meshes. The real metric terms used in this study to apply formula (19) on three-dimensional curvilinear meshes, forgotten here for a sake of clarity, are evaluated following the works Visbal and Gaitonde.²² Such a numerical treatment allows to handle some curvilinear

complex geometries, while preserving the numerical accuracy of the scheme. For the centered schemes

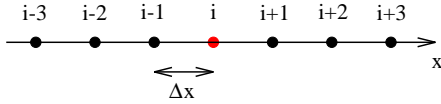


Fig. 11 Numerical discretization stencil

retained here, $a_0 = 0$, and $a_{-k} = a_k$. A sixth-order accurate scheme is reached by the use of three discrete points on each side of the central point i ($N = 3$), leading to a 7-point stencil. In this case, the values of the a_k retained in the following are: $a_1 = 45/60$; $a_2 = -9/60$; $a_3 = 1/60$. Some modification of these coefficients can also be found in literature, which allow for instance to preserve dispersion relation¹⁸ (DRP-schemes). Some compact schemes are also commonly used in literature,²³ which allow to reduce significantly the scheme stencil in each space direction. However, these last schemes are generally much more expensive than explicit schemes because they imply the resolution of a tridiagonal system at each space point. From our point of view, explicit schemes offer a better compromise between numerical cost and memory storage, and have thus been retained in this study.

To suppress high-frequency numerical instabilities due to the use of a non-dissipative centered scheme, a numerical filter has to be added to the simulation. This filtering operator F is applied to the solution vector V at each time step to damp the highest wavenumbers. At point i , the filtered quantity $F(\phi)$ of any variable ϕ is computed as:

$$F(\phi)_i = \sum_{k=-N}^N f_k \phi_{i+k} \quad (20)$$

where $f_{-k} = f_k$. For multidimensional configurations, the one-dimensional formula (20) is simply applied sequentially in each space direction. Various orders of filtering, depending on the stencil width (N) can be obtained. In the present case, a tenth-order accurate filter has been retained, with $N = 5$ leading to an 11-point discretization stencil. In this case, the values of the f_k are: $f_0 = 772/1024$; $f_1 = 210/1024$; $f_2 = -120/1024$; $f_3 = 45/1024$; $f_4 = -10/1024$; $f_5 = 1/1024$.

Simple application: 2D NACA0012 airfoil noise simulation

This section presents some early results dealing with the application of a full integrated strategy, combining CFD and aeroacoustic calculations simultaneously in a unique run. The case of the tone noise radiated by a NACA0012 airfoil with a sharp trailing edge at low incidence and low Reynolds number has been retained for this purpose.

The airfoil chord is set to $C = 0.3 \text{ m}$. The inflow velocity corresponds to a Mach number of 0.1. The Reynolds number, based on the chord and the inflow velocity is $Re = 200,000$. This low Reynolds number allows to carry out a Direct Numerical Simulation of the flow, which can be restricted to the 2D case since the flow remains laminar. The computation has thus been carried out in 2D only.

The airfoil is placed at an incidence of 4 degrees in the flow. Following Lawson et al.[31], this should lead to a tone noise emission at the trailing edge.

Figure 12 describes the different computational sub-domains that have been used for this study. The numerical schemes retained for the computation (both DNS and Euler) are: (i) a sixth-order centered space scheme combined with a 10th order filter; (ii) a third order explicit compact Runge-Kutta scheme for time integration.

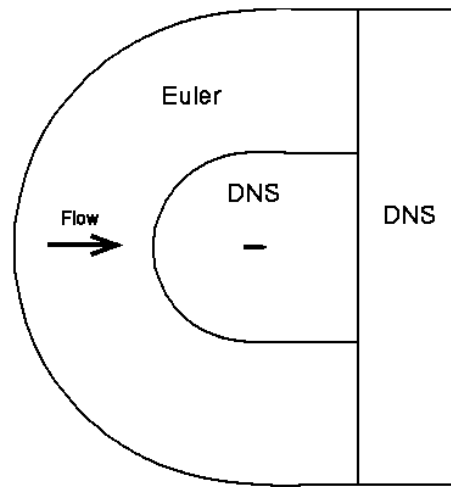


Fig. 12 Full computational domain, indicating the different solvers used during the integrated simulation

The computational domain is composed of three structured sub-domains: (i) a central one around the airfoil (2200×180 meshpoints), where a DNS is carried out to get an accurate description of the noise sources; (ii) an Euler sub-domain surrounding the central DNS zone (2200×64 meshpoints), which is used for midfield sound propagation computation; and (iii) a second DNS domain (30×488 meshpoints) placed downstream of the airfoil, which is used for both farfield sound propagation calculation and as an outflow zone for the airfoil's wake. This leads to a global mesh of 551,440 meshpoints. The wall-normal resolution of the main DNS grid has been set to ensure that approximately 40 points are located in the boundary layer. The highest frequency that can be handled by the mesh, in regard of the sixth-order space scheme is of the order of 2000 Hz in the far field. The global

computational domain used for this study extends to approximately 10 chords away from the profile.

A no-slip boundary condition is applied at the airfoil surface, and non-reflecting characteristic boundary are used for the far field. These boundary conditions have been generalized to five rows of ghostcells to be compatible with the 11-point space scheme.

To ensure the validity of the CFL stability constraint, the physical time step of the simulation has been set to $0.66 \mu s$. For the acoustic post-processing, a data-sampling has been performed every 25 time steps, meaning a storage sampling of $60 kHz$, with a useful frequency band of $30 kHz$.

Aerodynamic results show the establishment of a vortex shedding at the trailing edge, as it can be seen on figure 13 presenting isovalue contours of vorticity.



Fig. 13 Wake visualisation by isovalue contours of vorticity at the trailing edge

Noise emission and propagation is then investigated by the use of isovalue contours of the dilatation field Θ . Figure 14 shows an acoustic concentric wave pattern generated at the trailing edge, with an apparent wavelength of about 1.5 airfoil chord. It is clearly observed that the DNS solver is very well relayed by the Euler propagation solver, since no discontinuity of the acoustic waves is observed at the DNS/Euler coupling interface. This figure also indicates the dipolar nature of the noise source, which can thus be attributed to the scattering of the acoustic waves emitted by the vortex shedding on the trailing edge.

Finally, figure 15 displays the sound spectrum obtained at 30% chord above the trailing edge of the airfoil. It highlights the existence of a main dominant frequency of about $800 Hz$, together with its harmonic and sub-harmonic. This frequency is consistent with the apparent wavelength of the waves observed on figure 14.

Conclusions and Future Works

Some first accurate simulations of the turbulent 3D unsteady flow inside a slat cove of a high-lift wing have been performed by the use of a zonal hybrid RANS/LES approach. The results highlight the presence of several flow features, which are associated to aerodynamic noise emission. Such a complex simulation has been possible thanks to the use of a zonal

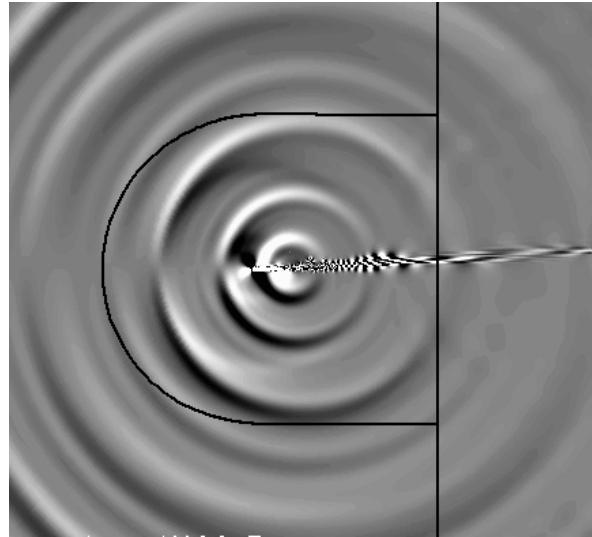


Fig. 14 Isovalue contours of the dilatation field Θ (range $\pm 0.3 m.s^{-2}$ black/white)

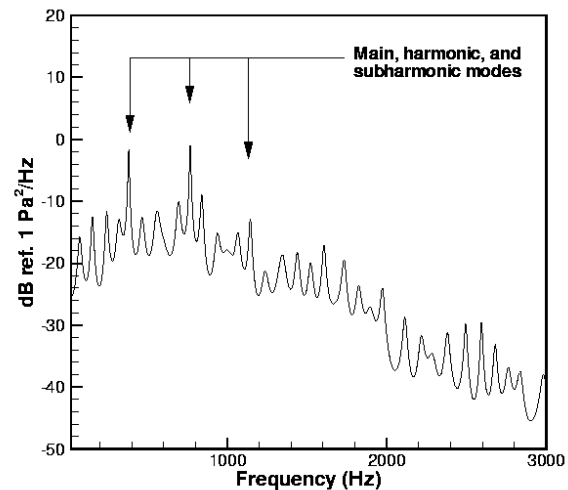


Fig. 15 Sound Pressure Level spectrum at 30% chord above the trailing edge of the airfoil

hybrid RANS/LES method, allowing to limit the cost of the simulation by reducing the extent of the LES zone.

In the second part of the paper, a full-integrated hybrid CFD/CAA process has been proposed and assessed on a simple NACA0012 configuration. This process is based on the coupling of an unsteady CFD zone, where the Navier-Stokes equations are solved, with a CAA propagation zone, where sound propagation through an inhomogeneous meanflow is simulated by resolving the Euler equations in a perturbation form.

In the future, a more precise analysis of the flowfield in the slat cove will be carried out, in order to get a

better understanding of the flow physics in such conditions. This appears to be a crucial point to be able to control and reduce the resulting noise emission. The local noise sources simulation will also be used as the first step of a hybrid CAA process, as the one proposed in the present paper, to compute the mid- and farfield noise generated by the high-lift device.

Acknowledgements

S. Ben Khelil is gratefully acknowledged for providing the 2D RANS result on the high-lift wing profile.

References

- ¹E. Manoha, C. Herrero, P. Sagaut, and S. Redonnet. Numerical prediction of airfoil aerodynamic noise. AIAA paper 2002-2573, 8th AIAA/CEAS Aeroacoustics Conference, Breckenridge, 17-19 June, 2002.
- ²M. Terracol, E. Manoha, C. Herrero, and P. Sagaut. Airfoil noise prediction using large eddy simulation, euler equations and kirchhoff integral. In *LES for Acoustics Workshop, Göttingen, Germany*, October 2002.
- ³E. Labourasse and P. Sagaut. Reconstruction of turbulent fluctuations using a hybrid RANS/LES approach. *J. Comput. Phys.*, 182:301–336, 2002.
- ⁴P. J. Morris, L. N. Long, A. Bangalore, and Q. Wang. A parallel three-dimensional computational aeroacoustics method using nonlinear disturbance equations. *J. Comput. Phys.*, 133:56–74, 1997.
- ⁵C. Hirsch. *Numerical computation of internal and external flow*, volume 2. J. Wiley and Sons, New York, 1990.
- ⁶T. J. Poinsot and S.K. Lele. Boundary conditions for direct simulations of compressible viscous flows. *J. Comput. Phys.*, 101:104–129, 1991.
- ⁷K. W. Thomson. Time dependant boundary conditions for hyperbolic systems. *J. Comput. Phys.*, 68:1–24, 1987.
- ⁸I. Mary and P. Sagaut. Large eddy simulation of flow around an airfoil near stall. *AIAA journal*, 40(6):1139–1145, 2002.
- ⁹M. Khorrami, B. Singer, and P. L. David. Time-accurate simulations and acoustic analysis of slat free shear layers : part ii. AIAA paper 2002-2579, 2002.
- ¹⁰M.J. Lighthill. On sound generated aerodynamically. I. general theory. *Proc. Roy. Soc. Lond.*, A 211:564–587, 1952.
- ¹¹M.J. Lighthill. On sound generated aerodynamically. II. turbulence as a source of sound. *Proc. Roy. Soc. Lond.*, A 222:1–32, 1952.
- ¹²E. Manoha, B. Troff, and P. Sagaut. Trailing edge noise prediction using large eddy simulation and acoustic analogy. *AIAA Journal*, 38(4):575–583, 2000.
- ¹³B.A. Singer, K.S. Brentner, D.P. Lockard, and G.M. Lilley. Simulation of acoustic scattering from a trailing edge. AIAA paper 99-0231, 37th Aerospace Sciences Meeting and Exhibit, Reno (NV), Jan. 12-15, 1999.
- ¹⁴B.A. Singer, D.P. Lockard, and K.S. Brentner. Computational aeroacoustic analysis of slat trailing-edge flow. *AIAA Journal*, 38(9):1558–1564, 2000.
- ¹⁵J.E. Ffowcs Williams and D.L. Hawkings. Sound generation by turbulence and surfaces in arbitrary motion. *Phil. Trans. Royal Soc.*, A 264:321–342, 1969.
- ¹⁶X. Gloerfelt, C. Bailly, and D. Juvé. Computation of the noise radiated by a subsonic cavity using direct simulation and acoustic analogy. AIAA paper 2001-2226, 7th AIAA/CEAS Aeroacoustics Conference, Maastricht (NL), May 28-30, 2001.
- ¹⁷E. Manoha, G. Elias, B. Troff, and P. Sagaut. Towards the use of boundary element method in computational aeroacoustics. AIAA paper 99-1980, 5th CEAS/AIAA Aeroacoustics Conference, Seattle, USA, 10-12 May, 1999.
- ¹⁸C. K. W. Tam and J. C. Webb. Dispersion-relation preserving finite difference schemes for computational acoustics. *J. Comput. Phys.*, 107:262–281, 1993.
- ¹⁹H.A. Grogger, J.W. Delfs, T.G. Lauke, M. Lummer, and J. Yin. Simulation of leading-edge noise of airfoils using caa based on body-fitted grids. 7th International Congress on Sound and Vibration, Garmisch-Partenkirchen, Germany, 4-7 July, 2000.
- ²⁰H.A. Grogger, M. Lummer, and T.G. Lauke. Simulating the interaction of a three-dimensional vortex with airfoils using caa. AIAA paper 2001-2137, 7th AIAA/CEAS Aeroacoustics Conference, Maastricht (NL), May 28-30, 2001.
- ²¹S. Redonnet, E. Manoha, and P. Sagaut. Numerical simulation of propagation of small perturbations interacting with flows and solid bodies. AIAA paper 2001-2223, 7th AIAA/CEAS Aeroacoustics Conference, Maastricht (NL), May 28-30, 2001.
- ²²M. R. Visbal and D. V. Gaitonde. Computation of aeroacoustic fields on general geometries using compact differencing and filtering schemes. AIAA paper 99-3706, 1999.
- ²³S. K. Lele. Compact finite difference schemes with spectral-like resolution. *J. Comput. Phys.*, 103:16–42, 1994.